Direct Space-to-Time Pulse Shaping at 1.5 μm

Jason D. McKinney, *Member, IEEE*, Dong-Sun Seo, and Andrew M. Weiner, *Fellow, IEEE*

***Abstract*—We present a novel direct space-to-time pulse shaper, operating in the 1.5-μm optical communications band which enables generation of continuous optical pulse sequences at a rate of ~ 100 GHz. The apparatus includes several novel features, such as the use of a diffractive optical element for spatial patterning, fiber coupled input/output, and a telescopic configuration which collectively enable generation of nearly equal amplitude optical pulse sequences over a time aperture in excess of 100 ps. We also present a mathematical description of the temporal and frequency modulation behavior of our apparatus, in addition to continuous 100-GHz optical pulse sequences generated in our system.**

***Index Terms*—Optical packet generation, pulse shaping, space-to-time conversion, ultrafast optics.**

I. Introduction

TECHNIQUES for generation of high-rate arbitrary optical pulse sequences could benefit many applications including coherent control, optical communications, optical computing, and microwave photonics. Specifically, for optical communications applications, e.g., optical packet generation, direct space-to-time pulse shaping [1] has been demonstrated to be a straightforward procedure by which to generate these pulse sequences. In this paper, we present recent advances in direct space-to-time pulse shaping in the 1.5-μm optical communications wavelength band.

Initially demonstrated by Froehly *et al.* with picosecond pulse durations [2]–[4], direct space-to-time (DST) pulse shaping was brought into the femtosecond regime by Leaird and Weiner [1] in the latter half of the 1990s. Thorough analysis of the pulse-shaping apparatus has been performed and generation of high-rate optical pulse sequences at Ti:sapphire wavelengths has been demonstrated [1], [5]. Chirp control in the apparatus has also been presented [6]. In this work, we present our recent experiments in DST pulse shaping in the 1.5-μm lightwave band. Here we introduce, for the first time to our knowledge, a novel DST pulse shaper operating in the lightwave communication band in a fiber-coupled configuration allowing generation of optical pulse sequences over a time aperture ≥ 100 ps. We present a theoretical description of the system operation, a novel technique for spatial pattern generation in the pulse shaper, and continuous optical pulse sequence generation at rates of 100 GHz enabled by our apparatus.

Previous work in our group [1], [5], [6] performed at Ti:sapphire wavelengths, while providing the fundamental description of the pulse shaping apparatus on a femtosecond time scale, also exhibited several areas which could be further engineered to enhance the overall system performance, particularly in the areas of pulse-shaping time aperture and equalization of pulses in the pulse-shaper output. For example, the available pulse shaping window in these experiments was limited to ~ 40 ps, as determined by the spatial patterning and sampling slit used in the shaper. Here, through a telescopic approach, we extend the pulse-shaping time aperture to greater than 100 ps, allowing compatibility with high-repetition-rate sources of comparable pulse period [7] and enabling us to move toward the generation of continuous pulse sequences at rates of ~ 100 GHz. Additional novel features, including advances in spatial patterning and reduction of polarization dependence, are also demonstrated. While we have demonstrated applications of our novel pulse shaper to arbitrary millimeter-wave electromagnetic waveform generation [8], [9], this work represents the first comprehensive description of the pulse-shaping apparatus itself.

In Section II, we describe our 1.5-μm DST pulse shaper and the novel features allowing generation of nearly equal amplitude optical pulse sequences over a time aperture of greater than 100 ps. Included in this discussion will be our new spatial patterning technique and a brief description of the diffractive optical elements used as the basis for our spatial patterns. The major system changes—the inclusion of a telescope within the pulse shaper and fiber coupling of the system—will be treated mathematically in Section III and supporting experimental data will be shown. Additionally in Section III, we will discuss new chirp behavior and control resulting from the fiber-coupled telescopic configuration. In Section IV, we will present generation of 100-GHz optical data from our DST shaper, and in Section V we will conclude.

II. Telescopic Fiber-Coupled DST Pulse Shaper

The goal of DST pulse shaping is the generation of reprogrammable high-rate optical pulse sequences. Fourier transform pulse shaping [10] is a commonly accepted method for generating nearly arbitrarily shaped optical waveforms, including high-rate pulse sequences. Despite the success of Fourier transform shaping, however, the method suffers from the complexity of calculating the requisite Fourier transform when generating high-rate pulse sequences in real time. This complexity is removed in DST pulse shaping where there exists a direct mapping from a spatially patterned short-pulse input to the time-domain optical waveform. Functionally, the DST shaper acts as

Manuscript received June 30, 2003; revised August 24, 2003. This work is supported by or in part by the U.S. Army Research Office under Contract DAAD19-00-0497, the National Science Foundation under Grant 0100949-ECS, and by Intel. The work of D. S. Seo was supported by the Korea Science and Engineering Foundation under Grant R01-2000-000-00249-0 and the Integrated Photonics Technology ERC, Inha University, Korea.

J. D. McKinney and A. M. Weiner are with the School of Electrical and Computer Engineering, Purdue University, West Lafayette, IN 47907-2035 USA (e-mail: mckinnjd@ecn.purdue.edu).

D.-S. Seo is with the School of Electrical and Computer Engineering, Purdue University, West Lafayette, IN 47907-2035 USA, on leave from Myongji University, Korea.

Digital Object Identifier 10.1109/JQE.2003.819542

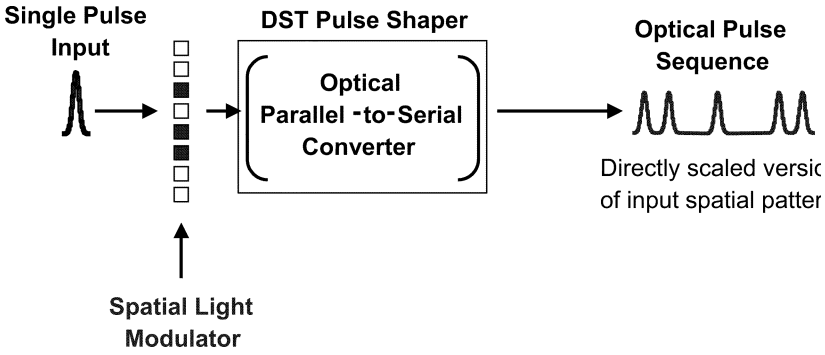

Fig. 1. Optical parallel-to-serial conversion in the DST pulse shaper. The pulse-shaper temporal output is a directly scaled version of a spatially patterned short-pulse input.

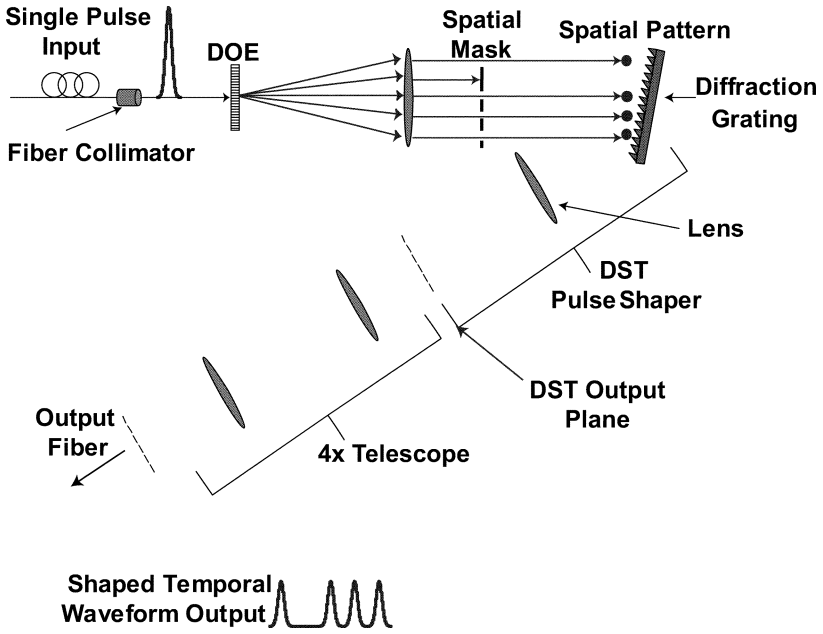

Fig. 2. The 1.5-μm telescopic fiber-coupled DST pulse shaper. Our pulse shaper includes fiber-coupled input/output and use of DOEs to achieve spatial patterning. A telescope has been added after the basic DST pulse shaper to broaden the achievable pulse-shaping time aperture.

an optical parallel-to-serial converter for a spatially patterned short-pulse input as illustrated schematically in Fig. 1. The temporal output of the shaper is controlled through simple manipulation of the applied spatial pattern at the pulse-shaper input.

In this work, we demonstrate significant improvements upon the basic grating–lens–slit implementation of the DST pulse shaper. In previous work, the pulse-shaping time aperture is limited by the finite size of the slit used to sample the pulse shaper output and the free-space system is not easily compatible with optical fiber-based systems. Additionally, the use of an amplitude mask and cylindrically focused input beam led to roll-off effects in the measured temporal output of the pulse shaper. We have included several novel features in our current DST pulse shaper to address these concerns.

We have moved this work to the 1.5-μm optical communication wavelength band, where a variety of fiber-based sources are available to be used as the input to our pulse shaper. Specifically, we aim for an apparatus compatible with high-repetition-rate sources, such as picosecond sources operating at 10 GHz, which will allow generation of continuous optical pulse sequences at rates in the 100-GHz range. To this end, we demonstrate the apparatus illustrated in Fig. 2. The output from an erbium fiber laser—either a passively mode-locked source producing $\sim$ 100-fs pulses at 50 MHz [11] or a 10-GHz, 1-ps actively mode-locked source [7]—is collimated with a fiber-pigtailed collimating lens and used as the input to our system. After collimation, the short-pulse input beam is spatially patterned via a diffractive optical element and subsequent spatial mask and the resulting spatial pattern is used as the pulse-shaper input. A 600-l/mm low-polarization-dependent loss (PDL) diffraction grating and 15-cm focal length achromat lens form the basis for the pulse shaper. The use of a low PDL diffraction grating in the system reduces the system PDL to $\sim$ 0.1 dB. This enables the pulse-shaping operation to be achieved without the need to explicitly control the polarization of the system input. This is an attractive feature given the polarization-modifying behavior of the single-mode optical fiber comprising the source, amplifiers, and measurement apparatus in our system. A $4\times$ telescope is inserted between the output plane of the basic DST shaper and the output single-mode optical fiber which replaces the thin slit used in previous work [1], [5], [6]. The high-rate optical pulse sequences from our

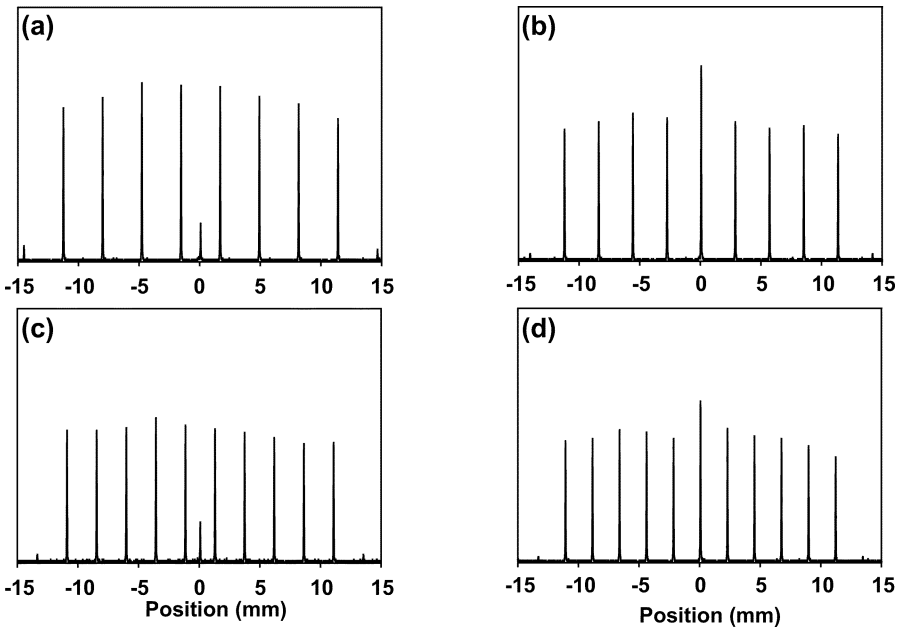

Fig. 3. Spatial profilometer measurements of representative DOE patterns, just prior to the diffraction grating in our apparatus. (a) Eight-spot pattern. (b) Nine-spot pattern. (c) Ten-spot pattern. (d) Eleven-spot pattern. The spatial patterns of (a) and (c) utilize the odd-order diffraction spots from the DOEs. The patterns of (b) and (d) utilize the even-order diffraction spots of the DOEs.

apparatus are measured via intensity cross correlation with a reference pulse directly from the input laser source.

Since the temporal output of the shaper is a directly scaled version of the applied spatial pattern at the input to the pulse shaper, any variation in the applied input pattern is exhibited by the output temporal waveform. When an amplitude mask is used to pattern a cylindrically focused Gaussian beam [1], [5], [6], the temporal waveform from the pulse shaper clearly shows a Gaussian roll-off due to the Gaussian nature of the illuminating input beam. In addition, any portion of the input beam which is blocked by the mask results in decreased system throughput. To achieve nearly equal-amplitude temporal features and increase the patterning efficiency of our pulse shaper, spatial patterning is now accomplished using diffractive optical elements (DOEs) [12]. These devices provide periodic spatial patterns which are further manipulated using an amplitude mask, allowing either periodic optical pulse sequences or optical data to be generated in the pulse shaper.

Our DOEs (custom devices, INO, Quebec, Canada) are binary, phase-only masks designed to divide the power from a single input beam equally into multiple output beams. These DOEs function as one-dimensional (1-D) spot generators and produce patterns ranging from 8 to 21 spots, providing a variety of input patterns for our pulse shaper. Examples of several DOE patterns are shown in Fig. 3. The patterns of Fig. 3(a) and (c)—eight and ten spots, respectively—are generated from the odd-order diffraction spots of the DOE. The small zeroth-order diffraction spot at $x = 0$ is most likely due to an error in phase step in our elements and can be blocked from the pulse-shaper input if so desired. Alternatively, patterns based on the even diffraction orders may be used, as illustrated by the nine and eleven spot patterns of Fig. 3(b) and (d). In these patterns, the slight amplitude difference in the zeroth order ($x = 0$) is again attributed to an error in phase step. If so desired, this spot may be attenuated to decrease the intensity to a level equal to that of the other spots in the pattern.

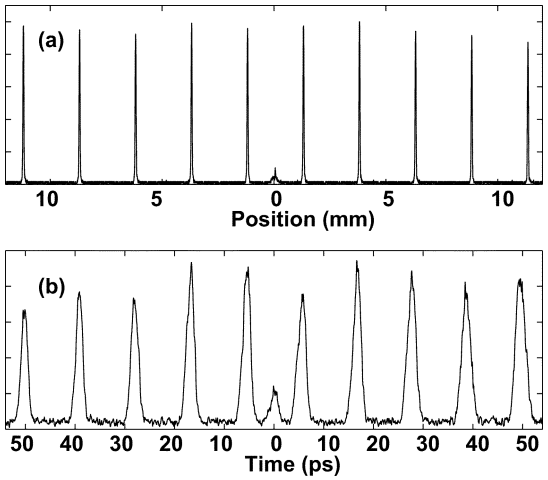

Fig. 4. Example of space-to-time mapping. (a) Ten-spot spatial pattern just before the diffraction grating. The spot-to-spot spacing is ~ 3.5 mm. (b) Optical cross correlation of the DST output for the pattern shown in (a). Given the space-to-time conversion constant of ~ 3.1 ps/mm and the spatial pattern above, the result is a ~ 92-GHz optical pulse sequence.

As is clearly illustrated, the DST shaper input consists of a series of nearly equal-intensity spots, effectively removing the time-aperture effect. Subsequent to the DOE, individual spots in the periodic patterns may be blocked to create optical data packets or otherwise desirable input patterns. Fig. 4 clearly illustrates the mapping from space to time. The bottom trace shows the pulse shaper output which consists of a series of ten pulses at ~ 92 GHz as determined by the space-to-time conversion constant of ~ 3.1 ps/mm and the ~ 3.5-mm spot spacing in the

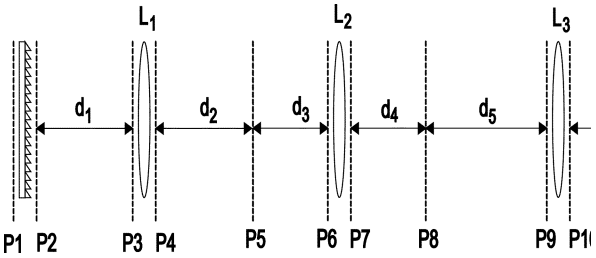

Fig. 5. System used for diffraction analysis. The primary planes of interest are P_5 and P_{11} which represent the DST shaper and telescope output planes, respectively.

input pattern. The optical pulse sequence of Fig. 4(b) clearly illustrates that the Gaussian temporal roll-off, previously incurred when amplitude masking a Gaussian beam to achieve spatial patterning [1], [5], [6], is removed when a DOE is used for this operation.

Our new spatial patterning technique removes time-aperture effects due to Gaussian illumination of an amplitude mask in previous work and increases the system patterning efficiency. We will now describe the effects of fiber coupling the pulse-shaper output and how inclusion of a telescope after the pulse shaper allows us to take full advantage of the equal-intensity spatial patterns generated by our diffractive optical elements. Combined, these features allow us to move toward generation of equal-amplitude optical pulse sequences over a time aperture $\geq$ 100 ps.

III. Mathematical Description of the DST Pulse-Shaping Apparatus

While the basic grating-lens-slit DST pulse shaper has been analyzed previously, the inclusion of a telescope after the shaper warrants reanalysis of several items of interest, namely the pulse shaping time-aperture and frequency modulation (chirp) behavior of the apparatus. To mathematically explain the effects of the additional telescope and fiber coupling of the shaper output, a diffraction analysis of the system similar to [1], [13] was performed. In this work, we present only the relevant results. The full diffraction analysis is contained in [14]. Fig. 5 shows the relevant system components and distances used in the diffraction analysis of our current system. We will begin this section with a discussion of the pulse shaping time-aperture which rigorously includes both the telescope following the shaper as well as the fiber coupling of the shaper output. We will then turn to the frequency modulation capability of the apparatus and discuss novelties arising due to the inclusion of the telescope.

A. Fiber Coupling and Pulse-Shaping Time Aperture of the Telescopic DST Pulse Shaper

Both the spatial extent of the user-defined spatial pattern applied to the pulse-shaper input and the size of the slit used to sample the shaper output equally affect the achievable pulse-shaping time aperture. To illustrate this, consider the pulse-shaper output, as expressed in [1], for a DST shaper constructed with an arbitrarily shaped output slit $a(x/x_o)$

$$e_{\text{out}}(t) \propto e_{\text{in}}(t) * \left[m\left(-\frac{\alpha}{\gamma}t\right) \exp\left(-\frac{\alpha^2}{\gamma^2 w^2 t^2}\right) A\left(\frac{2\pi x_o}{\gamma\lambda f_1 t}\right)\right]. \quad (1)$$

In this expression, $e_{\text{in}}(t)$ is the short=pulse input to the system, $m(-\alpha t/\gamma)$ is the applied spatial input pattern evaluated as a function of time, the Gaussian exponential term represents the intensity distribution of the Gaussian beam to which the spatial pattern is applied, and $A(2\pi x_o t/\gamma\lambda f_1)$ is the spatial Fourier transform of the slit function evaluated as a function of time. Here, the width of the applied spatial pattern is determined by the width of the Gaussian exponential (w) and x_o allows scaling of the slit function width. The astigmatism (α) and dispersion (γ) of the diffraction grating are given by

$$\alpha = \frac{\cos\theta_i}{\cos\theta_d} \quad (2)$$

$$\gamma = \frac{\lambda}{cd\cos\theta_d} \quad (3)$$

where λ is the system center wavelength, c is the speed of light, d is the period of the diffraction grating, and θ_i, θ_d are the incident and diffracted angles of the system input beam, respectively. The space-to-time conversion constant γ/α is then

$$\frac{\gamma}{\alpha} = \frac{\lambda}{cd\cos\theta_i}\left(\frac{\text{ps}}{\text{mm}}\right). \quad (4)$$

For our system, $\lambda = 1550$ nm, $d = 1.67$ μm, and $\theta_i = 12^\circ$ resulting in a space-to-time conversion constant of $\gamma/\alpha \approx 3.1$ ps/mm.

In the mathematical treatment of [1], the focus is on the interplay between the duration of the applied spatial pattern as determined by the width of the Gaussian in (1) and the time-aperture defined by Fourier transform of the sampling slit, $A(2\pi x_o t/\gamma\lambda f_1)$. From an efficiency standpoint then, the width of the slit should be chosen to allow generation of the desired waveform $m(-\alpha t/\gamma)$, while maintaining the highest possible system throughput, i.e., the slit is no smaller than necessary. In our current work, we aim to generate equal-amplitude pulse sequences which span a fixed time aperture of $\sim$ 100 ps. By employing DOEs to perform the requisite spatial patterning, the Gaussian amplitude variation of the spatial pattern is effectively removed. Thus, the Gaussian in (1) is removed, and the spatial extent of the input pattern is included in $m(-\alpha t/\gamma)$. Taking this into account, the time-domain output of the DST pulse shaper is given by

$$e_{\text{out}}(t) \propto e_{\text{in}}(t) * \left[m\left(-\frac{\alpha}{\gamma}t\right) A\left(\frac{2\pi x_o}{\gamma\lambda f_1}t\right)\right]. \quad (5)$$

For equal-amplitude pulse sequences, provided the correct spatial pattern is applied to the pulse shaper input, the available pulse-shaping time-aperture is effectively determined by the size of the slit used to sample the pulse-shaper output. Thus, to achieve equal-amplitude pulse sequences from the pulse shaper, the time-aperture effect of sampling the pulse-shaper output must be minimized.

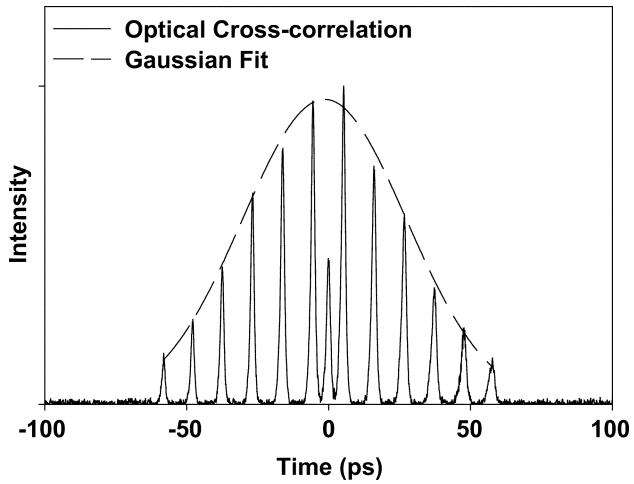

Fig. 6. Optical pulse sequence, spanning $\sim$ 120 ps, clearly showing the limited pulse-shaping time aperture due to the finite fiber mode size. The dashed curve is a Gaussian fit to the data exhibiting a $\sim$ 68-ps intensity FWHM.

Since we have replaced the variable slit used in previous work [1], [5], [6] with a single-mode optical fiber, the spatial width (x_o) of the "slit," and hence the available pulse-shaping time aperture, are now fixed. To illustrate, we model the single-mode fiber as a Gaussian with a $1/e$ beam waist equal to the effective mode-field radius of the fiber. Mathematically, the slit function $a(x/x_o)$ and its Fourier transform are now expressed as

$$a\left(\frac{x}{x_o}\right) = \exp\left(-\frac{x^2}{x_o^2}\right) \tag{6}$$

$$A\left(\frac{2\pi x_o}{\gamma\lambda f_1}t\right) = \exp\left(-\frac{\pi^2 x_o^2}{\gamma^2\lambda^2 f_1^2}t^2\right). \tag{7}$$

The intensity full-width at half-maximum (FWHM) of the pulse-shaping time aperture, as determined by the finite fiber mode size is then determined from the exponential of (7) to be

$$T = \sqrt{2\ln 2}\frac{\gamma\lambda f_1}{\pi x_o}. \tag{8}$$

When evaluated using our system parameters of $f_1 = 15$ cm, $\lambda = 1550$ nm, $d = 1.67$ μm, $\theta_i = 12°$, and $x_o = 5.25$ μm the predicted pulse-shaping time aperture is $T \approx 76$ ps.

To illustrate the effect of the fiber mode, consider Fig. 6. In this case, a spatial pattern consisting of 12 equal-intensity spots is applied to the pulse shaper input. With a space-to-time conversion constant of $\gamma/\alpha \approx 3.1$ ps/mm, the temporal output is a series of 12 pulses with a $\sim$ 10-ps spacing, yielding a temporal duration of $\sim$ 120 ps. Ideally, the equal-intensity spatial spots at the pulse-shaper input should map to equal amplitude pulses in time; however, the outer pulses are clearly seen to be attenuated due to the time aperture of the fiber mode. The measured intensity FWHM of the data of $\sim$ 68 ps, found by performing a Gaussian fit to the pulse sequence data (dashed curve), shows good agreement with the $\sim$ 76-ps duration predicted by (8). To alleviate this time-aperture effect, we place a telescope between the output of the basic DST pulse shaper and the single-mode fiber, which effectively broadens the time aperture due to the fiber by a factor of the telescope magnification.

In a general sense, the DST pulse shaper behaves as a spectrometer with a short-pulse input [1]. The size of the slit, or in our current shaper a single-mode optical fiber, defines the spectral resolution in this spectrometer. As the spectral resolution degrades, the available pulse shaping time aperture decreases. This can be visualized as spectrally slicing the short-pulse input to generate a longer output pulse from the apparatus—the narrower the sampling slit, the higher the spectral resolution, and the broader the pulse shaping time aperture. If we desire to increase the pulse-shaping time aperture (increase the spectral resolution of our spectrometer), we need to either increase the size of the spectral features at the pulse-shaper output or decrease the fiber mode size. In practice, it is easier to achieve the former by either changing the pulse-shaping lens (L_1 in Fig. 5) or by adding a telescope between the DST shaper and the output fiber. To illustrate this, take the spectrum of the pulse shaper, prior to fiber coupling (plane P_5 in Fig. 5), given by

$$E_{\text{out}}(x,\omega) \propto E_{\text{in}}(\omega)\, M\left(\frac{2\pi}{\lambda f_1\alpha}x - \frac{\gamma}{\alpha}\omega\right). \tag{9}$$

Here, $E(\omega)$ is the spectrum of the short-pulse input, M is the Fourier transform of the applied spatial pattern m, and the Gaussian exponential is the Fourier transform of the time aperture defined by the input beam size. The spectral feature size can clearly be increased by increasing the focal length f_1 of the pulse-shaper lens. This is impractical, however, in that a factor of 4 or more increase in spectral feature size would require a focal length of 60 cm or more for our shaper, leading to a pulse shaper on the order of 120 cm in length. The same increase in feature size can be achieved, with less increase in the pulse-shaper dimensions, if a telescope of appropriate magnification is placed between the pulse shaper and the output fiber. To illustrate the effect of the telescope on the pulse-shaper output, reconsider Fig. 5. The telescope, the portion of the system between plane P_5 and plane P_{11}, is now included in the diffraction analysis. For those familiar with field calculations utilizing the Fresnel diffraction integral, it is clear that the distances d_2, d_3 and d_4, d_5 do not need to be treated separately. In our analysis, these distances have been treated separately to facilitate expressing the fields in the system as a series of spatial Fourier transforms and quadratic phases arising from the position of each lens in the system. In the case of a perfectly aligned telescope, the only effect is a spatial scaling of the field at the telescope input. In this case, the spectrum after the telescope, prior to fiber coupling (plane P_{11} in Fig. 5), is

$$E_{\text{out}}(x,\omega) \propto E_{\text{in}}(\omega)\, M\left(-\frac{f_2}{f_3}\frac{2\pi}{\lambda f_1\alpha}x - \frac{\gamma}{\alpha}\omega\right) \tag{10}$$

where the spectrum, compared to (9), is clearly reversed and scaled by the magnitude of the telescope magnification f_3/f_2. To see the effect of scaling the spectrum on the time-domain field, we need only find the field coupled to the fiber by evaluating the overlap integral between the fiber mode and the field from the telescopic DST and take the inverse temporal Fourier transform

$$e_{\text{out}}(t) \propto e_{\text{in}}(t) * \left[m\left(-\frac{\alpha}{\gamma}t\right) A\left(\frac{f_2}{f_3}\frac{2\pi x_o}{\gamma\lambda f_1}t\right)\right]. \tag{11}$$

Several items of interest are contained in (11). First, the addition of the telescope does not affect the space-to-time mapping. The relation between space at the input and time at the output is still

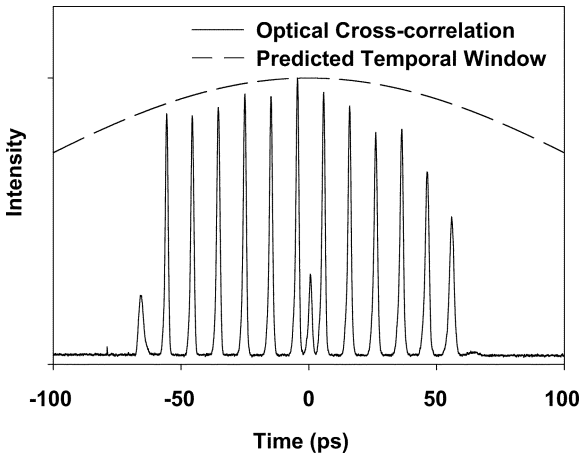

Fig. 7. Inclusion of a 4 × telescope effectively broadens the pulse-shaping time aperture of our pulse shaper to ~ 303 ps.

given by $t = -\gamma x/\alpha$. Additionally, the effective size of the fiber mode has also been decreased by a factor of the inverse of the telescope magnification. This brings the fiber closer to the ideal δ-function slit [1], where the pulse-shaping time aperture is completely defined by the applied spatial input pattern. If we now evaluate the fiber mode using the same Gaussian form of (6), the pulse-shaping time aperture defined by the fiber is now given by

$$A\left(\frac{f_2}{f_3}\frac{2\pi x_o}{\gamma\lambda f_1}t\right) = \exp\left(-\frac{f_2^2}{f_3^2}\frac{\pi^2 x_o^2}{\gamma^2\lambda^2 f_1^2}\right). \tag{12}$$

Here, the time aperture of the fiber mode is clearly broadened by a factor of the telescope magnification f_3/f_2, with the intensity FWHM window now given by

$$T = \sqrt{2\ln 2}\frac{f_3}{f_2}\frac{\gamma\lambda f_1}{\pi x_o}. \tag{13}$$

Fig. 7 shows the effect of the telescope on the system functionality quite clearly. With a 4 × telescope, the window has been broadened to $T \approx 303$ ps, enabling nearly equal-amplitude pulses over the central ~ 120 ps. We note that there is some distortion of the pulses occurring later in time. We believe this is related to the large diffraction angle ($\sim 46°$) which leads to only the central portion of the diffraction grating being exactly a focal distance away from the pulse-shaping lens L_1, which is not included in the analysis.

Broadening of the pulse-shaping time aperture is one clear effect of the addition of a telescope after the pulse shaper. The chirp, or frequency modulation, of the pulse shaper is also modified and will now be addressed.

B. Frequency Modulation in the DST Pulse Shaper

Previous work has shown that, when the DST shaper is appropriately configured, the system imparts a quadratic temporal phase, or frequency modulation, onto the output temporal waveform [1], [6]. The key is that not only is the amplitude of the applied spatial pattern is mapped to time, but any phase curvature—arising, for example, from a converging or diverging input to the system—is as well. Since it is this quadratic spatial phase which gives rise to a frequency modulation of the pulse-shaper output, the positions of the pulse shaping and telescope lenses may also lead to a spatial phase curvature. This enables us to tune the applied frequency modulation by positioning the system lenses appropriately. In this discussion, we will demonstrate how the inclusion of the telescope provides additional control over frequency modulation in the system, as compared to previous work [6]. In addition, we predict previously unnoticed changes in the pulse-shaping time aperture when the system is configured to impose a frequency modulation.

In the above treatment, the pulse shaper was assumed to be in a zero applied frequency modulation, or "chirp-free," configuration where all distances in Fig. 5 are set to the appropriate focal length, i.e., $d_1 = d_2 = f_1, d_3 = |f_2|$, $d_4 + d_5 = f_2 + f_3$, and $d_6 = f_3$. If we now allow some or all of these distances to vary, we are able to impose a controlled frequency modulation onto the pulse-shaper output waveforms. This behavior is desirable in some situations, either to eliminate the effects of a diverging or converging input beam to the DST shaper or to impose a controlled frequency modulation onto the temporal output of the shaper to be utilized in other experiments [15]. Specifically, in this work, we allow the distances d_1, d_2, and d_6 to vary, with all other distances set to the appropriate "chirp-free" positions as detailed above. When this variation is included in the analysis, subject to the conditions $d_1 + d_2 = 2f_1$, $d_3 = |f_2|$, and $d_4 + d_5 = f_2 + f_3$ the chirp, or frequency modulation in nm/ps, imposed by the pulse shaper is given by

$$\frac{\partial\lambda}{\partial t} = \frac{\lambda}{c\gamma^2}\left[\frac{\alpha^2}{R} + A_1\frac{f_1 - d_2}{f_1^2} + \frac{A_1^2}{A_2}\frac{f_2 - d_3}{f_1^2} + A_3\frac{A_1^2}{A_2^2}\frac{f_2^2}{f_3^2}\frac{f_3 - d_6}{f_1^2}\right] \tag{14}$$

where

$$A_1 = \frac{f_1^2}{f_1 d_1 + (2f_1 - d_1)(f_1 - d_1)} \tag{15}$$

$$A_2 = \frac{f_2^2}{f_2(d_3 + d_4) - d_3 d_4} \tag{16}$$

$$A_3 = \frac{f_3^2}{f_3(d_5 + d_6) - d_5 d_6}. \tag{17}$$

In (14), the term α^2/R represents the contribution to the frequency modulation due to a noncollimated spatial pattern at the input of the DST shaper. In the case of a cylindrically focused Gaussian beam and amplitude mask, this term would represent the phase-front radius of curvature of the cylindrically focused Gaussian beam. In our system, this amounts to a series of Gaussian spots generated by the DOE where the spot spacing varies with propagation distance. This convergence/divergence has been modeled as a Gaussian beam with a phase front given by $\exp(-j\pi x^2/\lambda R)$. The terms A_1, A_2, and A_3 are unitless scaling factors arising from the positions of the pulse-shaping lens, telescope lenses, and output fiber. These represent a scaling of the spatial frequencies in the diffraction analysis. These scaling factors exhibit a maximum value of 1 when the pulse shaper is aligned in a "chirp-free" configuration and decrease as the aforementioned positions are changed.

From (14), it is clear that the frequency modulation in the shaper can be controlled through positioning not only the pulse shaping lens, but also the first telescope lens (d_3) as well as the

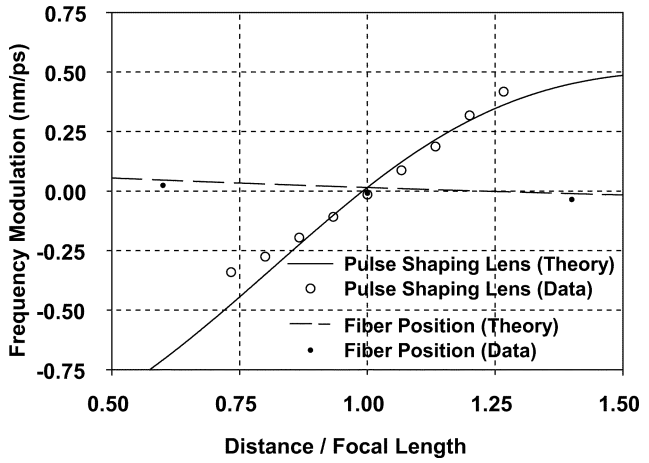

Fig. 8. Frequency modulation in our DST pulse shaper. The curves above illustrate the imposed frequency modulation as a function of pulse shaping lens (L_1 in Fig. 5) position and the location of the output fiber.

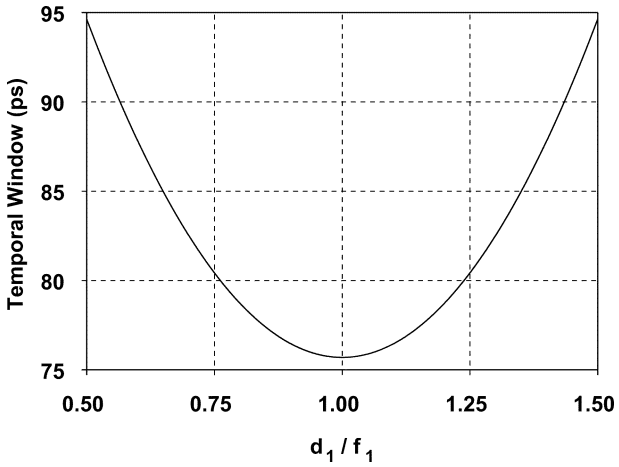

Fig. 9. Predicted broadening of the pulse-shaping time aperture as a function of pulse-shaping lens position.

output fiber position d_6. Frequency modulation in our apparatus is controlled by either movement of the pulse-shaping lens or by movement of the output fiber. Fig. 8 illustrates the imposed frequency modulation as a function of these two positions. This measurement was performed by generating two pulses, separated by ~ 90 ps, in the DST shaper and measuring the difference in center wavelength ($\Delta\lambda$) of these pulses as a function of pulse-shaping lens or output fiber position. The imposed frequency modulation, in nm/ps, is then calculated from $\Delta\lambda/90$ ps. In this figure, the abscissa is the distance which is varied divided by the respective "zero frequency modulation" or chirp-free position. For example, the solid curve illustrates the imposed frequency modulation as a function of the grating—pulse-shaping lens position d_1 divided by the pulse-shaping lens focal length f_1. For this curve, the distance d_2 is subject to the constraint $d_2 = 2f_1 - d_1$ and the telescope lenses are positioned such that $d_3 = |f_2|$, $d_4 + d_5 = f_2 + f_3$, and $d_6 = f_3$. In words, the telescope is perfectly aligned with the output fiber positioned in the telescope output plane and the pulse-shaping lens is moved longitudinally between the diffraction grating and telescope input plane. The dashed line shows the imposed frequency modulation as a function of the output fiber position d_6 divided by the focal length of the second telescope lens f_3. For this measurement, the pulse shaper is aligned with $d_1 = d_2 = f_1$, $d_3 = |f_2|$, and $d_4 + d_5 = f_2 + f_3$. The imposed frequency modulation due to movement of the pulse-shaping lens is found to vary much more rapidly than that due to movement of the output fiber, as is consistent with the inclusion of the telescope. The form of the imposed frequency modulation due to the pulse-shaping lens position agrees with that demonstrated previously [6]; however, there is now the more slowly varying modulation controlled by the output fiber position which may be utilized to fine-tune the imposed frequency modulation. The decreased sensitivity to the output fiber position is clearly shown by the last term in (14). Here, the variation of the frequency modulation with the output fiber position is clearly reduced by the square of the telescope magnification $(f_3/f_2)^2$. This is in contrast with the work of [6] where the position of the output slit had the largest effect on the imposed frequency modulation. The small offset from zero when the pulse shaper is in the chirp-free configuration (residual frequency modulation of ~ 0.015 nm/ps) is most likely due to a finite radius of curvature on the phase front of the applied spatial pattern and slight misalignments of the pulse-shaping lens (L_1) and first telescope lens (L_2).

When the pulse shaper is aligned to impose a frequency modulation on the shaper output, the pulse-shaping time aperture is predicted to broaden. Consider the intensity FWHM of the basic DST pulse-shaping time aperture given by (8). When the pulse shaper is aligned to impose a frequency modulation, as mentioned above the spatial frequencies in the diffraction analysis are scaled. Thus, f_1 is replaced with f_1/A_1. The intensity FWHM of the pulse shaping time aperture is now expressed as

$$T = \sqrt{2\ln 2}\frac{\gamma\lambda f_1}{\pi x_o A_1}. \tag{18}$$

As the pulse-shaping lens is moved in either direction from the chirp-free position of $d_1 = d_2 = f_1$, A_1 decreases from its maximum value of 1 leading to an increase in the width of the achievable pulse shaping time aperture. As the pulse-shaping lens position d_1 is numerically varied over a range of $.5f_1 \leq d_1 \leq 1.5f_1$ with $d_2 = 2f_1 - d_1$, while holding all other distances fixed at the appropriate chirp-free position, the pulse-shaping time aperture is predicted to vary from ~ 76 to ~ 95 ps FWHM, as illustrated in Fig. 9. Conceptually, this is once again explained using the aforementioned spectrometer analogy. As the pulse-shaping lens position is varied, the spectral features at the pulse-shaper output are no longer focused at the output fiber; the spectral feature size is now larger. Therefore, the output fiber appears smaller (closer to the ideal δ-function slit) and the pulse-shaping time aperture is accordingly broadened. This effect would also be predicted for the far-field, on-axis field of a DST shaper constructed with an arbitrarily shaped slit; however, in previous work [1], [13], the time aperture for the DST pulse shaper was only analyzed for the case of $d_1 = d_2 = f_1$.

While this behavior is clearly predicted from the diffraction analysis of the system, measurement of this phenomenon in our apparatus is quite difficult. The simplest measurement of this broadening would be to impose a large frequency modulation to the shaper output and perform a numerical Gaussian fit to

the optical cross-correlation measurement of the resulting optical pulse sequence. This is nonideal, however, in that the use of an optical pulse sequence spanning a $\sim$ 100-ps time aperture results in significant spectral broadening. The optical bandwidth in our system is limited to ~ 30 nm by our erbium-doped fiber amplifiers. Over the specified range of pulse-shaping lens position, the imposed frequency modulation varies between $\sim \pm 0.3$ nm/ps. The result is that pulses in this sequence are modulated near the edge of the optical spectrum and the entire sequence is temporally apertured by the optical spectrum of the amplifiers. In the end, this effect is quite difficult to separate from the predicted broadening of the pulse-shaping time aperture. Thus, this phenomenon stands as a prediction. Should one desire to measure this effect in the future, broad-band, gain-flattened amplifiers could be employed to remove spectral time-aperture effects.

IV. Continuous 100-GHz Optical Pulse Sequence Generation

The intended application for our system, while we have demonstrated applications in millimeter-wave and RF signal generation [8], [9], is optical packet generation at rates in excess of the current commercial single-channel state of the art of 40 GB/s. Several techniques with this aim have been demonstrated, for example, the interleaving of identical lower rate (i.e., 10 Gb/s) data streams common in optical time division multiplexing (OTDM) systems experiments [16], [17] and the use of fiber Bragg gratings [18], [19] to generate high-rate fixed pulse sequences. These techniques, however, suffer from strict synchronism requirements and lack reprogrammability, respectively, when considered for real systems. Generation of optical data packets spanning a 100-ps frame through DST pulse shaping, when combined with a source of comparable pulse period and high-speed modulator arrays, avoids both of these concerns. Reprogrammability is addressed through simple changes in the applied spatial pattern to the pulse shaper while synchronous operation is ensured through the physics of the pulse-shaping apparatus. In this section, we preset our work on generation of continuous optical pulse sequences at rates of 100 GHz, aimed at reprogrammable optical packet generation.

To lay the framework for these experiments, we should consider the operation of the pulse shaper with a low repetition-rate source. When the system input is a passively mode-locked fiber laser ($\sim$ 100 fs pulses at 50 MHz), each source pulse is converted to an optical pulse sequence in the shaper. These sequences span a $\sim$ 100-ps time aperture and repeat every 20 ns as determined by the source repetition rate. Thus, these are burst sequences and they are effectively isolated in time. Fig. 10 shows several periodic burst sequences generated in our shaper. Our DOEs, which define the periodic pulse sequences achievable from our shaper, are designed such that the overall sequence duration is fixed at $\sim$ 100 ps—regardless of the number of pulses in the sequence. By increasing the number of pulses in the sequence, the pulse period decreases, leading to a higher pulse rate within the packet, as illustrated in Fig. 10. Here, the pulse rate is changed simply by changing the DOE used to generate the sequence.

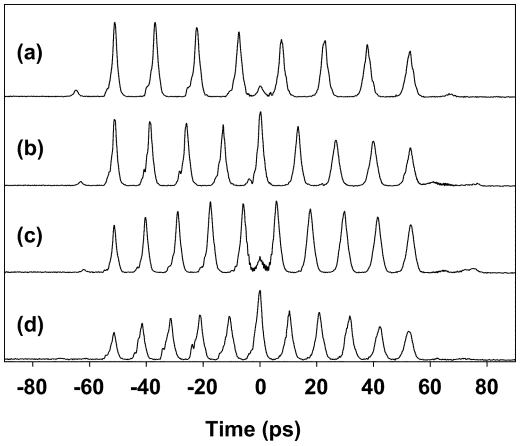

Fig. 10. Burst periodic pulse sequences from the DST pulse shaper. (a) Eight pulses at ~ 67 GHz. (b) Nine pulses at ~ 76 GHz. (c) Ten pulses at ~ 85 GHz. (d) Eleven pulses at ~ 96 GHz.

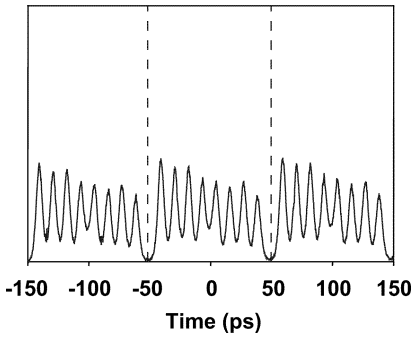

Fig. 11. The ~ 88-GHz optical pulse sequences. Here, each burst of eight pulses is generated from one source pulse, arriving every 100 ps. The stitching error at the frame boundaries (dashed lines) is a result of the mismatch between the source pulse period and the duration of the optical pulse sequence. Timing jitter in the source laser is seen to degrade the extinction between neighboring pulses in the optical cross-correlation measurement.

When the passively mode-locked erbium fiber laser [11] ($\sim$ 300-fs pulses, 50 MHz) is replaced with an actively mode-locked laser source [7] which provides $\sim$ 1-ps pulses at a rate of 10 GHz, one could envision stitching sequences generated from adjacent source pulses together to form continuous high-rate optical data. In the simplest case, this amounts to rate multiplying our 10-GHz source up to 100 GHz. To illustrate this concept, consider Fig. 11, which shows an optical cross-correlation measurement of a series of ~ 88-GHz optical pulse bursts. Here, each frame of eight pulses is generated from a single source pulse, with the boundaries between adjacent frames delineated by a dashed line.

The frames then repeat at the source repetition rate of 10 GHz. Fig. 11 clearly illustrates several key items which must be overcome in order to achieve truly continuous, high-quality optical data at rates of 100 GHz. First, there is an obvious stitching error between adjacent frames—for a continuous 100-GHz pulse train, we need the pulse-to-pulse spacing, as well as the frame-to-frame spacing, to be 10 ps. Additionally, the extinction between pulses is observed to be less than optimal. We remove the stitching error by changing the spatial input pattern to the shaper. By replacing the spatial pattern used to generate the above pulse sequence with one giving pulse

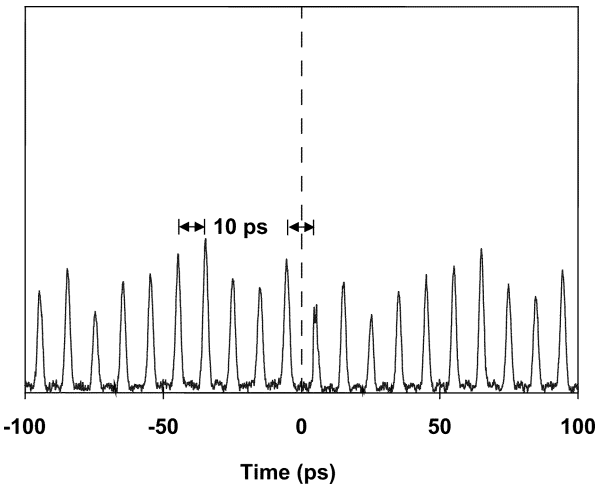

Fig. 12. Continuous 100-GHz pulse train. Compared to the pulse bursts illustrated in Fig. 11, the stitching error between frames has been minimized through proper choice of the optical pulse sequence duration. Additionally, reduction in the source timing jitter (< 200 fs from ~ 1.4 ps) gives 100% extinction between pulses.

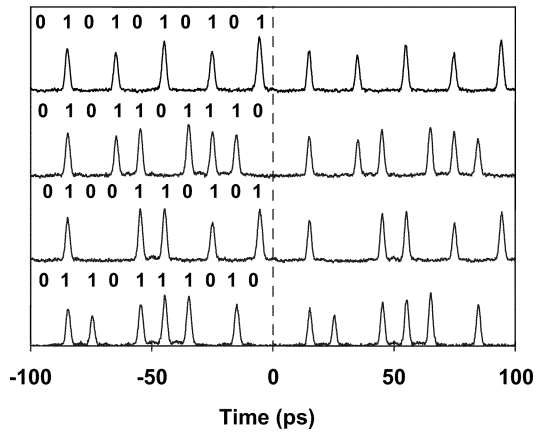

Fig. 13. The 100-GHz optical data. Data packets spanning 100 ps, with pulse rates of 100 GHz, are generated from each source pulse. The optical data is arbitrary within each frame (dashed lines) and is repeated at the source repetition rate. Incorporation of a high-speed optoelectronic modulator array would allow reprogramming on a frame-by-frame basis.

sequences exhibiting 10-ps pulse spacing after space-to-time conversion, we obtain a continuous 100-GHz optical pulse train as shown in Fig. 12.

While we believe our apparatus should not contribute any timing jitter to our pulse sequences, jitter in the source laser is found to degrade the extinction in the cross-correlation measurements of our pulse sequences. In Fig. 12, the extinction is observed to be 100%, due to minimization of timing jitter in our 10-GHz source, which has been reduced from ~ 1.4 ps to less than 200 fs. The amplitude fluctuations apparent in the pulse train of Fig. 12 are artifacts of slight misalignment of the output fiber and are, hence, repeated within each ~ 100-ps pulse sequence (frame) from the shaper. To alleviate these fluctuations for applications, a more sensitive alignment mechanism for the output fiber could be used. An additional item of interest is that the chirp of an individual pulse in these sequences is determined almost entirely by the input laser source ($e_{\rm in}(t)$ in (5), with negligible contribution from the pulse-shaping apparatus. Provided the input source is chirp-free, additionally dispersion compensation of these pulse sequences prior to transmission is not necessary.

To encode optical data onto this pulse train, we need only alter the spatial pattern applied to the pulse shaper input. To keep the overall pulse rate, we block individual spots in the input spatial pattern used to generate the pulse train of Fig. 12. Examples of optical data generated in this manner are shown in Fig. 13. The data within a single frame, again separated by the dashed lines, is arbitrary and repeats at the source repetition rate. To achieve electronic control over the data within a frame, we note the fixed mask could be replaced with a spatial light modulator, such as a liquid crystal modulator frequently employed in Fourier pulse shaping experiments [10] or high-speed optoelectronic modulator array, allowing the spatial pattern and, hence, pulse-shaper output to be altered via computer control. With the inclusion of high-speed optoelectronic modulator arrays operating at the source repetition rate of 10 GHz (currently under development), individual pulses in the 100-GHz sequence could be modulated at the somewhat slower rate of 10 GHz, enabling optical data to be reprogrammed on a frame-by-frame basis. This would allow generation of truly independent optical data at rates of 100 Gb/s and beyond, determined solely by the applied spatial pattern and density of parallel modulators in the array.

V. Conclusion

We have presented a novel direct space-to-time pulse shaper operating in the 1.5-μm lightwave communications band. Our apparatus generates nearly equal-amplitude optical pulse sequences, over a pulse-shaping time aperture exceeding 100 ps, at pulse rates of ~ 100 GHz. A telescopic configuration is used to broaden the available pulse-shaping time aperture defined by the output fiber and time-aperture effects in the spatial patterning process are removed by the use of a diffractive optical element for spatial pattern generation. Incorporation of a 10-GHz source as the system input allows continuous 100-Hz optical pulse sequence generation. Our apparatus, if combined with high-speed optoelectronic modulator arrays, could allow optical packet generation at data rates of approximately 100 GHz—more than twice the current commercial single-channel state of the art.

References

[1] D. E. Leaird and A. M. Weiner, "Femtosecond direct space-to-time pulse shaping," *IEEE J. Quantum Electron.*, vol. 37, pp. 494–504, 2001.

[2] B. Colombeau, M. Vampouille, and C. Froehly, "Shaping of short laser pulses by passive optical fourier techniques," *Opt. Commun.*, vol. 19, pp. 201–204, 1976.

[3] P. Emplit, J. P. Hamaide, F. Reynaud, C. Froehly, and A. Barthelemy, "Picosecond steps and dark pulses through nonlinear single mode fibers," *Opt. Commun.*, vol. 62, pp. 374–379, 1987.

[4] P. Emplit, M. Haelterman, and J. P. Hamaide, "Picosecond dark soliton over a 1-km fiber at 850 nm," *Opt. Lett.*, vol. 18, pp. 1047–1049, 1993.

[5] D. E. Leaird and A. M. Weiner, "Femtosecond optical packet generation by a direct space-to-time pulse shaper," *Opt. Lett.*, vol. 24, pp. 853–855, 1999.

[6] ——, "Chirp control in the direct space-to-time pulse shaper," *Opt. Lett.*, vol. 25, pp. 850–852, 2000.

[7] T. F. Carruthers and I. N. Duling III, "10-GHz, 1.3-ps erbium fiber laser employing soliton pulse shortening," *Opt. Lett.*, vol. 21, pp. 1927–1929, 1996.

[8] J. D. McKinney, D. E. Leaird, and A. M. Weiner, "Millimeter-wave arbitrary waveform generation with a direct space-to-time pulse shaper," *Opt. Lett.*, vol. 27, pp. 1345–1347, 2002.
[9] J. D. McKinney, D. S. Seo, and A. M. Weiner, "Photonically assisted generation of continuous arbitrary millimeter electromagnetic waveforms," *Electron. Lett.*, vol. 39, pp. 309–311, 2003.
[10] A. M. Weiner, "Femtosecond pulse shaping using spatial light modulators," *Rev. Sci. Instrum.*, vol. 71, p. 1929, 2000.
[11] K. Tamura, H. A. Haus, and E. P. Ippen, "Self-starting additive pulse modelocking erbium fiber ring laser," *Electron. Lett.*, vol. 28, pp. 2226–2228, 1992.
[12] J. N. Mait, "Design of binary-phase and multiphase fourier gratings for array generation," *J. Opt. Soc. Amer. A*, vol. 7, pp. 1514–1528, 1990.
[13] D. E. Leaird, A. M. Weiner, S. Shen, A. Sugita, S. Kamei, M. Ishii, and K. Okamoto, "High repetition rate femtosecond wdm pulse generation using direct space-to-time pulse shapers and arrayed waveguide gratings," *Opt. Quantum Electron.*, vol. 33, pp. 811–826, 2001.
[14] J. D. McKinney, "Direct space-to-time pulse shaping and applications in arbitrary electromagnetic waveform generation," Ph.D. dissertation, Purdue Univ., West Lafayette, IN, 2003.
[15] J. D. McKinney, D. S. Seo, D. E. Leaird, and A. M. Weiner, "Photonically assisted burst and continuous arbitrary millimeter waveform generation via direct space-to-time pulse shaping," in *Ultrafast Electronics and Optoelectronics*, 2003, OSA Tech. Dig., Opt. Soc. Amer., pp. 109–112.
[16] S. Kawanishi, "Ultrahigh-speed optical time-division-multiplexed transmission technology based on optical signal processing," *IEEE J. Quantum Electron.*, vol. 34, pp. 2064–2079, 1998.
[17] M. Nakazawa, T. Yamamoto, and K. R. Tamura, "Ultrahigh-speed otdm transmission beyond 1 terabit-per-second using a femtosecond pulse train," *IEICE Trans. Electron.*, vol. E85-C, pp. 117–125, 2002.
[18] P. Petropoulos, M. Ibsen, M. N. Zervas, and D. Richardson, "Generation of a 40-GHz pulse stream by pulse multiplication with a sampled fiber Bragg grating," *Opt. Lett.*, vol. 25, pp. 521–523, 2000.
[19] J. Lee, P. The, Z. Yusoff, M. Ibsen, W. Belardi, T. Munro, and D. Richardson, "A holey fiber-based nonlinear thresholding device for optical cdma receiver performance enhancement," *IEEE Photon. Technol. Lett.*, vol. 14, pp. 876–878, 2002.

Jason D. McKinney (M'03) received the Ph.D. degree from Purdue University, West Lafayette, IN, in 2003.

His research is in the area of optical space-time processing and RF photonics—specifically, optical pulse shaping for arbitrary electromagnetic waveform generation. From July 2001 through May 2003, he was a Graduate Assistant in Areas of National Need (GAANN) Fellow sponsored by the U.S. Department of Education. Dr. McKinney is currently a Visiting Assistant Professor of Electrical and Computer Engineering at Purdue University.

Dr. McKinney is a Member of the Optical Society of America. In 2002, he was a finalist for the Optical Society of America/New Focus Student Award and in 2003 he received the Chorafas prize for outstanding doctoral research from the Dimitris N. Chorafas Foundation, as well as the Motorola Student Excellence Award for academic merit and leadership. He has also received numerous awards in recognition of his teaching ability and is an Associate Fellow of the Purdue University Teaching Academy.

Dong-Sun Seo received the B.S. and M. S. degrees in electronic engineering from Yonsei University, Korea, in 1980 and 1985, respectively, and the Ph. D. degree in electrical engineering (optoelectronics) from the University of New Mexico, Albequerque, in 1989.

From 1980 to 1986, he was with the Agency for Defense Development as a Research Engineer. From 1986 to 1990, he was a Research Assistant and later a Research Staff member at the Center for High Technology Materials, University of New Mexico. In 1990, he joined the faculty of Myong-Ji University, Korea, where he is currently a Professor in the Department of Electronics. From 1994 to 1995, he was a Visiting Research Fellow at the Photonics Research Laboratory, University of Melbourne, Australia. Since 2002, he has been with Purdue University, West Lafayette, IN, as a Visiting Research Professor in the School of Electrical and Computer Engineering. His current research interests are in the areas of very-high-speed optical data generation and transmission, semiconductor lasers, microwave photonics, and optical CDMA.

Andrew M. Weiner (S'84–M'84–SM'91–F'95) received the Sc.D. degree in electrical engineering from the Massachuetts Institute of Technology (MIT), Cambridge, in 1984.

From 1979 through 1984, he was a Fannie and John Hertz Foundation Graduate Fellow at MIT. In 1984, he joined Bellcore, at that time one of the premier research organizations in the telecommunications industry. In 1989 he was promoted to Manager of Ultrafast Optics and Optical Signal Processing. He moved to Purdue University, West Lafayette, IN, in 1992 as Professor of Electrical and Computer Engineering and is currently the Scifres Distinguished Professor of Electrical and Computer Engineering. From 1997 to 2003, he served as ECE Director of Graduate Admissions. His research focuses on ultrafast optical signal processing and high-speed optical communications. He is especially well known for pioneering the field of femtosecond pulse shaping, which enables generation of nearly arbitrary ultrafast optical waveforms according to user specification. He has published four book chapters and over 120 journal articles. He has been author or coauthor of over 200 conference papers, including approximately 60 conference invited talks, and has presented over 50 additional invited seminars at universities or industry. He holds 5 U.S. patents.

Prof. Weiner is a Fellow of the Optical Society of America. He received numerous awards for his research, including the Hertz Foundation Doctoral Thesis Prize (1984), the Adolph Lomb Medal of the Optical Society of America (1990), awarded for pioneering contributions to the field of optics made before the age of thirty, the Curtis McGraw Research Award of the American Society of Engineering Education (1997), the International Commission on Optics Prize (1997), the IEEE LEOS William Streifer Scientific Achievement Award (1999), the Alexander von Humboldt Foundation Research Award for Senior U.S. Scientists (2000), and the inaugural Research Excellence Award from the Schools of Engineering at Purdue (2003). He has served on or chaired numerous research review panels, professional society award committees, and conference program committees. In 1988–1989, he served as an IEEE Lasers and Electro-optics Society (LEOS) Distinguished Lecturer. He was General Co-Chair of the 1998 Conference on Lasers and Electro-optics, Chair of the 1999 Gordon Conference on Nonlinear Optics and Lasers, and Program Co-chair of the 2002 International Conference on Ultrafast Phenomena. In addition, he has served as Associate Editor for IEEE JOURNAL OF QUANTUM ELECTRONICS, IEEE PHOTONICS TECHNOLOGY LETTERS, and *Optics Letters*. He has served as an elected member of the Board of Governors of IEEE LEOS from 1997 to 1999 and as Secretary/Treasurer of IEEE LEOS from 2000 to 2002. He is currently a Vice President (representing IEEE LEOS) of the International Commission on Optics (ICO).